Science Arts & Métiers (SAM)

is an open access repository that collects the work of Arts et Métiers Institute of Technology researchers and makes it freely available over the web where possible.

Effect of Weld Travel Speed on Solidification Cracking Behavior. Part 1: Weld Metal Characteristics

N. Coniglio [a] and C.E. Cross [b]

[a] Laboratory of Mechanics, Surface and Materials Processing (MSMP-EA7350), 2 cours des Arts et Métiers, 13617 Aix-en-Provence – France. Email : nicolas.coniglio@ensam.eu. Phone : 0033 4 4293 8183.

[b] Los Alamos National Laboratory (LANL), Los Alamos, NM (United States)

A. ABSTRACT

Solidification cracking is a weld defect common to certain susceptible alloys rendering many of them unweldable. It forms and grows continuously behind a moving weld pool within the two-phase mushy zone and involves a complex interaction between thermal, metallurgical and mechanical factors. Research has demonstrated the ability to minimize solidification cracking occurrence by using appropriate welding parameters. Despite decade's long efforts to investigate weld solidification cracking, there remains a lack of understanding regarding the particular effect of travel speed. While the use of the fastest welding speed is usually recommended, this rule has not always been confirmed on site. Varying welding speed has many consequences both on stress cells surrounding the weld pool, grain structure, and mushy zone extent. Experimental data and models are compiled to highlight the importance of welding speed on solidification cracking. This review is partitioned into three parts: Part I focuses on the effects of welding speed on weld metal characteristics, Part II reviews the data of the literature to discuss the importance of selecting properly the metrics, and Part III details the different methods to model the effect of welding speed on solidification cracking occurrence.

Keywords: solidification cracking; welding; welding speed; crack initiation; crack growth.

B. NOMENCLATURE

h	Plate thickness
s	Travel speed

t	Time
x	Direction of heat source displacement
BTR	Brittle Temperature Range
CET	Columnar-to-Equiaxed Transition
CSZ	Crack Susceptible Zone
G	Temperature gradient
H	Heat input
I	Welding current
K	Thermal conductivity
LHC	Linear Heat Content
Q	Welding power
R	Solidification growth rate
R_i	Radius of weld cross-section
SCTR	Solidification Cracking Temperature Range
T	Temperature
U	Welding voltage
α	Thermal diffusivity
ε	Strain
$\dot{\varepsilon}$	Strain rate
ξ	Traveling coordinates
η	Welding efficiency

C. INTRODUCTION

Solidification cracking is a commonly encountered defect during welding, especially in high-sulfur steels, austenitic steels, and aluminum alloys. Solidification cracks form due to a complex interplay of mechanical, thermal, and metallurgical factors. Their formation is strongly dependent on both material composition and welding parameters. To increase productivity, fabricators aim at reducing manufacturing time by increasing welding speed. This commonly implies using laser and electron-beam welding processes that involve welding speeds (10^1-10^2 mm.s^{-1}) faster than commonly encountered in arc welding processes (10^0-10^1 mm.s^{-1}). However, while the use of fastest travel speeds in arc welding to avoid solidification cracking has been commonly accepted, it seems not to always apply for the faster speeds encountered during beam welding that can lead to numerous weld bead defects [1,2] including solidification cracking itself.

Solidification cracking, described by Campbell as "an uniaxial tensile failure in weak materials" [3], appears at the solidification end inside a mushy zone that is subjected to tensile strains. The microstructure forms in the solidification zone, referred to as the mushy zone, located at the rear of the melting zone and bordered by two isothermal surfaces corresponding to liquidus and solidus temperatures. The semi-solid in the mushy zone has little ductility in the terminal stage of solidification, when the liquid fraction is no longer high enough for grains to move around and rearrange in order to accommodate tensile strains. When liquid feeding cannot adequately

compensate solidification shrinkage and thermal contraction of the mushy zone, solidification cracking occurs along grain boundaries.

Solidification by epitaxial growth of columnar grains is generally observed in welding from the border of the fusion zone to the center due to high thermal gradients. However, equiaxed dendritic grains can also form in the center area of the fusion zone. A susceptible zone in-between coalescence and coherency does exist in which solidification cracking may possibly form (Figure 1). The coalescence temperature corresponds to the minimum solid fraction so that the mushy zone has a mechanical resistance to shearing, usually induced by dendrite entanglement. The coherency temperature is the temperature at which the first solid bridges form in-between grains leading to a mechanical resistance in tension.
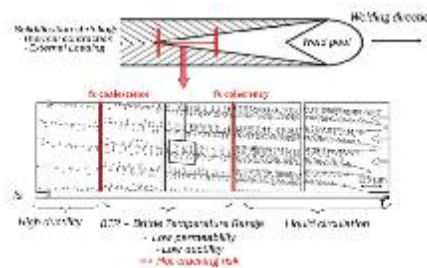

Figure 1 Schematic representation of solidification cracking in a columnar structure [4]

The hot cracking temperature range, also referred to as Brittle Temperature Range (BTR) and Solidification Cracking Temperature Range (SCTR), relates to the interval of temperatures over which solidification cracking is likely to occur. It is usually associated to the coalescence-to-coherency range. It is argued that a large solidification range permits a large build-up of strain and a greater likelihood to crack [5]. It is also believed that the faster the welding speed is conducted, the faster the cooling rate and the less time the weld is exposed to thermal strains with the BTR. Moreover, crack growth speed being fixed by welding speed, fast welding speeds tend to reduce cracking susceptibility as the crack tip cannot be continuously maintained in the mushy zone but this valuable effect is countered by the limited time available for backfilling the thermal strain-induced opening of the mushy zone.

Little research work has been reported in the literature on the relationship between travel speed and solidification cracking. The Part I of the present work focuses on reviewing the particular effect of welding speed on weld metal characteristics. The observations deal with metallurgical, thermal, and welding conditions, which change when varying travel speed.

D. GRAIN STRUCTURE

Grain structure and thus weld texture is affected by the travel speed as the weld pool shape is elongated at fast welding speeds. Grain boundaries are oriented preferentially perpendicular to the isotherms. Therefore, the shapes of the isotherm lines (and in particular the liquidus) that are dependent on the welding process parameters influence the grain structure.

I.   Ferrous alloys

Ferrous alloys are sensitive to the welding speed in regards to their susceptibility to solidification cracking. Incompletely melted grains in the partially-melted zone are nucleation sites from which weld metal may crystallize. The direction of the consequent epitaxial growth is aligned with the maximum temperature gradients that are perpendicular to the isotherms. Faster welding speeds are accompanied by altered weld pool size and shape and modified microstructural textures. With the increase in welding speed, the weld pool changed from an elliptical shape (Figure 2 a) to a teardrop shape (Figure 2 b)because of the deformed isotherms (change in heat flow) and the increased undercooling delaying the solidification process [6]. Both experimental work [7] [8] [9] [10] and simulations [6] correlate the weld pool shape to the grain texture and the tear drop shape to the formation of a continuous centerline grain boundary.

At slow welding speeds, an elliptical shaped pool is generated (Figure 2 a). The associated elliptical shape of the isotherms promotes curved macroscopic patterns with a competitive growth favoring grains with Miller indices 100 direction nearly parallel to the maximum temperature gradient [8]. The welding joint contains curved grains from the side to the center due to the continuous curvature of the isotherms. Indeed, a columnar grain which survives over any great distance in an elliptical weld pool exhibits considerable curvature due to the progressive change in the favored growth direction [9]. The crack susceptibility is low due to the tortuous path that would have to follow solidification cracking during its growth.

In case of fast welding speeds, the weld pool elongates with the shape of isotherm lines close to straight lines near the weld pool (Figure 2 b). The tear-drop shaped weld pool has an almost invariant direction of maximum thermal gradient at all points on the weld pool edge from the fusion boundary to the weld center [9]. This thermal field geometry results in any grain favorably oriented for growth at the fusion boundary being able to grow at optimum speed (competitive growth) in the direction of maximum gradient, i.e. perpendicular to the trailing edge [8]. Grains grow straight from side to center and meet at mid-way of the weld width without interacting with adjacent grains. As solidification cracks often form preferentially along the weld centerline [10], the presence of straight, long, and continuous centerline grain boundaries are harmful for crack resistance. Indeed, these long continuous grain boundaries along the weld are a preferential location for macro-segregation of sulfur and phosphorous (two elements that lower the solidus temperature, maintain liquid films at the boundaries and lengthen the BTR) therefore increasing

solidification cracking susceptibility. The microstructure tends to adopt at higher velocity an orientation normal to the weld direction [6]. It must be noticed that the dendrites are assumed to be aligned perfectly in a direction perpendicular to the growth front. However, in reality, dendrites have preferred crystallographic growth directions and cannot bend in the temperature field. As growth competition occurs, the grains oriented the closest to the growth direction are selected to minimize undercooling.
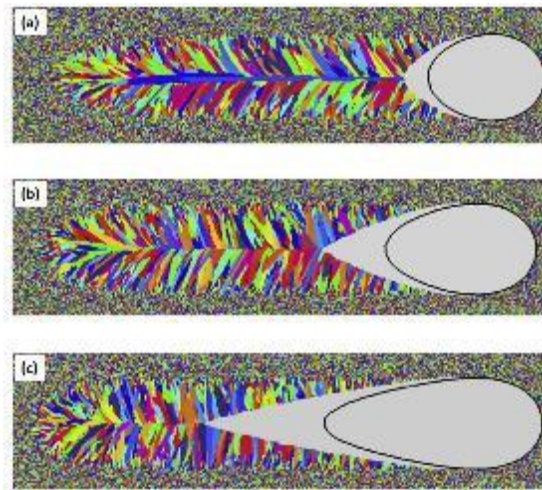

Figure 2 Simulated grain structure of URANUS 2202 welds made by GTAW process using a 3D coupled cellular automaton – finite element model. Welding speed and power are (a) 1 mm·s^{-1} and 4500 W, (b) 2 mm·s^{-1} and 7500 W, (c) 5 mm·s^{-1} and 15000 W. Welding power is adjusted to keep the weld width unchanged [6].

II.   Nickel-based alloys

Nickel-based alloys are widely used in various industry facilities due to their high corrosion resistance, hardness and high strength at elevated temperature. However these alloys are susceptible to solidification cracking [11–14][15]. EBSD observations reveal that solidification cracks propagate preferentially along two types of high-angle disoriented grain boundaries: solidification grain boundary (SGB) and solidification sub-grain boundary (SSGB) (Figure 3). Similar to ferrous alloys, the formation of a centerline grain boundary constitutes a potential weldability issue in regards to solidification crack formation because this last region to solidify is enriched in alloying elements and impurities that lower the solidus and thus lengthen the mushy zone.
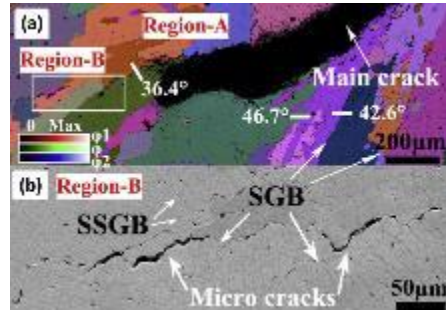
Figure 3 (a) EBSD and (b) SEM images of solidification crack in autogenous GTA weld of Ni-28W-6Cr alloy. SSGB and SGB referred to Solidification Sub-Grain Boundary and Solidification Grain Boundary, respectively [11].

Welding speed effect on the formation of centerline grain boundary was investigated experimentally and through modeling for autogenous GTA, IN718 superalloy welds on 2 mm-thick sheets [14]. Modeling the formation of a centerline grain boundary during welding required the coupling of models for heat transfer and dendritic growth in multicomponent alloys. Welding power and speed varied from 300 to 1900 W and from 2.5 to 15 mm·s^{-1}, respectively. The traditional and most common formulation of heat input (H in J.mm^{-1}) is given by:

$$H = \frac{Q}{s}$$
(Eq. 1)

, where Q is welding power (in W) and s is welding speed (in mm.s^{-1}). Accordingly, the weld pool shape and microstructure of the welded joint was mapped for variable effective power as a function of welding speed.

A sharp transition from circular to tear-drop shaped weld pools occurred at a threshold heat input of approximately 150 J.mm^{-1}. However, the tear-drop shape was not sufficient to form centerline grain boundaries. Indeed, the formation of centerline grain boundaries required both a tear-drop shaped weld pool (heat input below 150 J.mm^{-1}) and an effective power above 900 W [14]. These conclusions are summarized in a power-speed weldability map (Figure 4) and prove that centerline grain boundaries may be avoided in practice through the choice of a suitable combination of welding power and velocity.
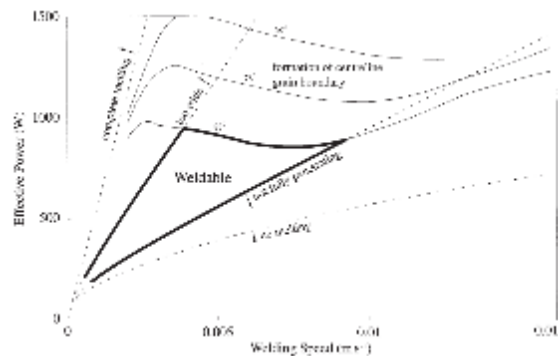
Calculations proved that centerline grain boundaries should not form even with a tear-drop shaped weld pool unless growth undercooling exceed a threshold value [14], in contrast to general understanding. The dominant effect of heat power is demonstrated by associating the formation of centerline grain boundary not to the undercooling distance alone (Δx_{und}) but to the ratio $\left(\frac{\Delta x_{und}}{\rho}\right)$, where Δx_{und} is the distance from the liquidus to the solidification front along the weld centerline and ρ is the curvature of the liquidus isotherm at the trailing edge of the weld pool [14]. For IN718 superalloy, the relationship between dendrite growth velocity v_{kin} and undercooling ΔT is given by [14]:

$$v_{kin} = 1.28 \cdot 10^{-7} \cdot \Delta T^{3.05}$$
(Eq. 2)

III. Aluminum alloys

Aluminum alloys have an ambiguous behavior in welding. Indeed with faster welding velocities, the susceptibility of stray grain formation at the weld centerline increases but is simultaneously in competition with the refinement tendency of the microstructure due to very high undercooling.

The solidification condition in the weld is controlled in part by the thermal gradient (G) and solidification growth rate (R) [4,16]. Thermal gradients (G) are minimum at the weld centerline and maximum on the weld side because of the large heat extraction along the colder base metal, thus inducing the elongation of the weld pool from circular to tear-drop shape at fast welding speeds. Assuming that dendrite solidification velocity corresponds to solidification growth rate due to competitive growth, solidification growth rate (R) is zero at the side interface and maximum at the center, accordingly:

$$R = s \cdot \cos(\alpha)$$
(Eq. 3)

, where s is welding speed and α is angle between solidification growth direction and welding direction.

The Columnar-to-Equiaxed transition (CET) has been associated to specific forms of thermal gradient-solidification rate relationships such as the solidification parameter $\frac{G}{R}$ [8]. Small $\frac{G}{R}$ ratios are associated with high constitutional undercooling ahead of the solid-liquid interface and equiaxed grain structures [17]. Hence equiaxed solidification tends to occur unaided in the centerline region of the weld pool, where solidification rates *(R)* are the highest and the thermal gradients *(G)* flattest due to the distance of the arc (Figure 5), and is generally associated to fast

7

welding speeds and important undercooling [9,16,18]. Columnar grain structure was always found predominantly at the weld interface where high $\frac{G}{R}$ ratios exist. The variation in both local solidification rate and thermal gradient in a single weld on moving around the fusion boundary from the side to the weld center causes a progressive change in solidification substructure across an individual weld bead [9].
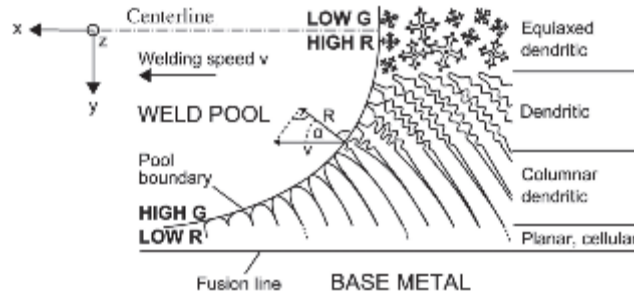

Figure 5 Variation in thermal gradient G, solidification growth rate R, and grain structure along solidification front in GTA weld pool (top-sectional view) [16].

The ambiguous behavior of aluminum alloy with travel speed is revealed by the existence of the most unsuitable welding velocity at intermediate values. Indeed, autogenous AA6060 GTA welds were investigated from 2 to 6 mm·s^{-1} with variation of current from 80 to 145 A to maintain a constant weld width. Large stray grains were observed above 4 mm·s^{-1} (Figure 6) causing a deterioration in solidification cracking resistance. Using the Controlled Tensile Weldability (CTW) test, the critical strain rate for solidification crack formation dropped from -0.06 to -0.20 %·s^{-1} when increasing welding speeds from 2 to 6 mm·s^{-1} [19].
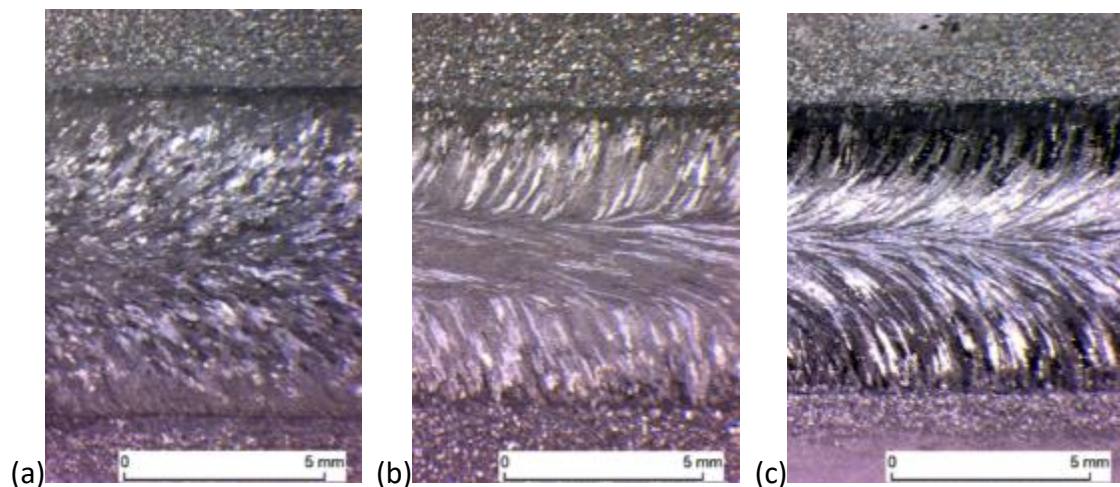

Figure 6 Grain structure at top surface of weld metal for autogenous AA6060 GTA welds at (a) 2 (b) 4 and (c) 6 mm·s^{-1} [19].

Faster welding velocities were investigated for autogenous GTA full-penetration welds on 3 mm-thick sheets of 1050A, 6082, and 5083 aluminum alloys [16]. The welding speed was varied

from 2 to 11.5 mm·s^{-1} and the current was adjusted between 170 and 200 A to maintain a constant full-penetrated weld bead size. Solidification cracks were prevented for welding speeds faster than 8 mm·s^{-1} (Figure 7), this threshold velocity corresponding to the minimum velocity for equiaxed grain formation along the weld centerline. The CET and associated grain refining effect has been proven experimentally [16,19–24][25–27] and numerically [25][28–32] to reduce efficiently the aluminum weld metal susceptibility to solidification cracking because of the better partitioning of the overall straining conditions [28,33] and the more tortuous paths to follow during crack growth (in comparison with straight columnar grain interfaces). Efficient grain refiners to avoid cracking in aluminum welds are Ti [21,23,24,34,35], Sc [21,35,36], B [23], TiB$_2$ [16,19], Zr [23,35,37], and even Mg for Al-Si alloys [38]. Moreover disturbance of the weld pool, e.g. by electromagnetic [9,39] or arc oscillated [40] stirring, avoids straight columnar grain formation, refines the grain structure, and subsequently lowers cracking susceptibility.
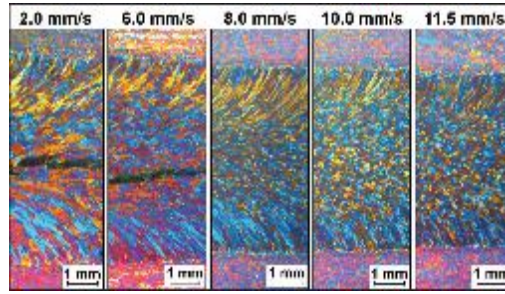

Figure 7 Weld metal grain structure and solidification crack formation for AA6082 GTA welds at different welding speeds [16].

E. Crack Susceptible Zone

The region susceptible to solidification cracking within the mushy zone is referred to as the Crack Susceptible Zone (CZS) (Figure 8) and is quantified by its length or by a range of temperature, either Brittle Temperature Range (BTR) [7,41–45] or Solidification Cracking Temperature Range (SCTR) [43]. The CSZ extends usually from the coherency (T_c) to the solidus (T_s) temperature range. The CZS length is calculated as the ratio of the temperature range from coherency T_c to solidus T_s with the temperature gradient G:

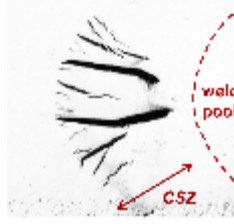$$CSZ = \frac{T_c - T_s}{G} = \frac{BTR}{G}$$

(Eq. 4)

Figure 8 Illustrated CSZ length measured in cracked mushy zone after Varestraint test.

Therefore an increase in welding speed should reduce the gradient *G* and subsequently elongate the CSZ length. Basic premise consists in associating longer distances (i.e. large CSZ) to more difficult feeding of shrinkage induced by longer and narrower interdendritic liquid channels associated with reduced permeability. Consequently, higher solidification cracking susceptibility is expected at faster welding speeds [12]. As fast travel speeds lengthen the mushy zone, it has been hypothesized that the experimentally-observed beneficial travel speed effect observed on cracking susceptibility may possibly be attributed to the dependency of strain on the heat flow condition [46].

The CSZ is measured usually from the lengths of the cracks form by rapidly-applied high strains, such as in Varestraint [47] and Trans-Varestraint tests [48][49]. Care must be taken in weldability testing based upon crack length as cracks form and continue to grow during the entire time of strain application [44,50], leading to errors in estimating these temperature-based indexes if strain is too slowly applied [51]. The length of the crack susceptible zone is usually measured as the length of the cracks generated during a fast-bending Varestraint test. The Varestraint test consists in bending quickly (within 0.1s) the weld joint during welding to induce high transverse tensile stresses and subsequently form solidification cracks "as long as the crack susceptible zone". The length of the crack susceptible zone is more accurately defined at slow welding speed, i.e. when the mushy zone is almost stationary during bending. The welding speed must be accounted for the calculation of the BTR length because the crack grows during the time of bending according to [41]:

$$L_W = L_B + L_F = L_B + s \cdot \frac{(\varepsilon_u - 2\varepsilon_{min})}{\dot{\varepsilon}}$$ (Eq. 5)

, where L_W is whole crack length, L_F is front crack length, L_B is back crack length (i.e. BTR), s is welding speed, ε_{min} is strain required for cracking, ε_u is given augmented strain, $\dot{\varepsilon}$ is strain rate. Therefore it is advised to have fast bending speeds. As the mushy zone continues moving during strain application of 0.4 and 17 mm for travel speeds of 4 mm.s^{-1} (GTAW) and 167 mm.s^{-1} (LBW), respectively, the BTR measurements are more accurate for slow welding speed processes. If using fast welding speeds, then a calculation must be performed to convert measured crack lengths in BTR and CSZ lengths. Therefore some works have focused on getting a better control of strain by standardizing the Transvarestraint equipment and methodology [52].

Care must be taken when converting the macroscopic bending strain ($\varepsilon = \frac{t}{2R}$ with t plate thickness and R radius of curvature of mandrel) to locally applied strain in the CSZ because simulations have demonstrated that strains are strongly localized in the trailing edge of molten pool during bending [42,44,50,53,54]. The local strains in the mushy zone can reach one order of magnitude greater than the average strain applied during bending [42,55–58].

One issue in investigating the welding speed effect is to isolate it. Welding speed may be varied while keeping the other parameters constant (i.e. constant welding power Q) but the weld joint size decreases with faster welding speeds. The power Q may also be increased simultaneously with the speed to maintain the weld size constant (i.e. $\frac{Q}{s}$ ratio constant). For autogenous GTA welds of low alloy steels, iso-geometries of weld joints are obtained by varying welding speed s (mm.s^{-1}) and welding current I (A) accordingly [59]:

$$I = 38 + 25s \qquad\qquad\qquad \text{(Eq. 6)}$$

Varying welding speed and current according to Eq. 6 showed that the CSZ as measured with the Varestraint test increases at fast welding speeds (Figure 9). This suggests that increasing welding speed deteriorates solidification crack resistance when maintaining wled bead shape constant [59]. Moreover, alloys with high solidification range show longer CSZ and associated higher solidification cracking susceptibility.
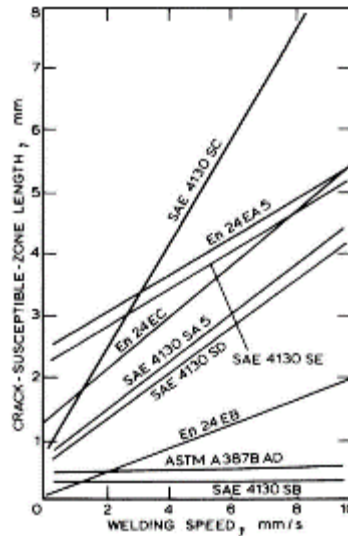

Figure 9 CSZ lengths measured using Varestraint test at constant bead width by increasing current and welding speed according to the relationship $I = 38 + 25s$ [59].

The theoretical calculation of the temperature distribution around a moving heat source has been performed to investigate the elongation of isotherms with welding speed. Many complex models have been proposed to simulate isotherms around a weld pool [60][61,62] but only the

point heat source (i.e. Rosenthal model) is presently used to illustrate weld speed effect. In fact, all models will provide similar qualitative trends but the most complex models should lead to more precise quantitative results. The Rosenthal model is applied in 2D or 3D in correlation with heat flow modes away for the weldment.

The Rosenthal formula estimates the temperature distributions around a punctual moving heat source. For a given material, the BTR range is defined as the interval between an upper (T_1) and lower (T_2) temperatures. Applying the 2D Rosenthal model (Figure 10) to calculate the length of the CSZ (referred to as the distance x) demonstrates that the length of the CSZ related to the pre-defined BTR depends on the $\frac{Q}{s}$ ratio:

$$x = \xi_1 - \xi_2 = \pi \alpha \frac{Q^2}{s} \left(\frac{1}{2\pi Kh}\right)^2 \left[\frac{1}{(T_2 - T_0)^2} - \frac{1}{(T_1 - T_0)^2}\right]^2 \qquad \text{(Eq. 7)}$$

, where (ξ_1, ξ_2) are traveling coordinates ($\xi = x - s \cdot t$), t is time, α is thermal diffusivity, K is thermal conductivity, h is plate thickness.
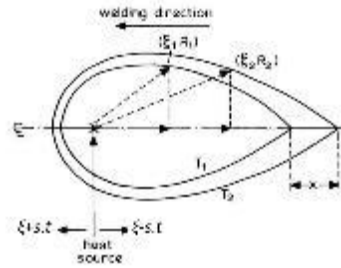

Figure 10   Coordinates used for Rosenthal calculations

If considering only that the microstructural tendency for cracking is associated with the liquid channel length to be fed, this equation corresponding to full-penetration welding condition shows that at constant Q, increasing s reduces the CSZ and therefore reduces the susceptibility to cracking. However, increasing s and maintaining $\frac{Q}{s}$ ratio constant implies an increase in $\frac{Q^2}{s}$ and subsequently longer CSZ and higher susceptibility to cracking. This calculation agrees with experimental evidences (recall Figure 9). Applying Eq. 7 specifically to low alloy steels (properties listed in Table 2) leads to the following relationship plotted in Figure 12 [59]:

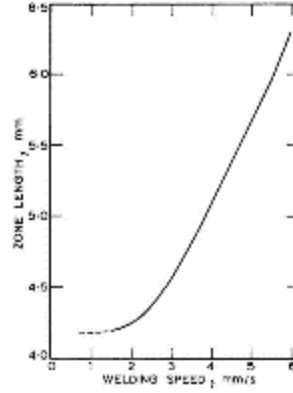$$CSZ = \frac{0.02(1 + 12s + 36s^2)}{s} \qquad \text{(Eq. 8)}$$

Figure 11   CSZ theoretical length as a function of welding speed for low alloy steel welds according to Eq. 8 and Table 1 [59]

Table 1   low alloy steel properties used to calculate CSZ length in Eq. 8 and Fig. 12 [59].

Properties	Values
Current I (A)	38+25·s
Heat input Q (J·mm^{-1})	$\eta \cdot U \cdot I$
Tension U (V)	11
Welding efficiency η	0.40
Lower temperature of CSZ T_2 (°C)	1000
Upper temperature of CSZ T_1 (°C)	1500
Sheet thickness h (mm)	2
Thermal conductivity K (cal·cm^{-1}·s^{-1})	0.1
Thermal diffusivity α (cm²·s^{-1})	0.2

Partial-penetration welds are simulated using the 3D Rosenthal model. Similar calculations applied to the 3D Rosenthal model for a point heat source show that the length of the CSZ does not depend on welding speed s [60]:

$$x = \xi_1 - \xi_2 = \frac{Q}{2\pi K}\left[\frac{1}{(T_2-T_0)} - \frac{1}{(T_1-T_0)}\right] \tag{Eq. 9}$$

Eq. 9 demonstrates that, for partial penetration welds, increasing s at constant Q does not change the CSZ and therefore does not affect the susceptibility to cracking. However, increasing s while maintaining $\frac{Q}{s}$ ratio constant means that the welding power Q is increased leading to longer CSZ and higher susceptibility to cracking.

In summary, Rosenthal modeling correlates the length of CSZ to Q in full-penetration welds (3D Rosenthal model) and $\frac{Q^2}{s}$ in partial penetration welds (2D Rosenthal model). The time t_s within the CSZ, i.e. to drop temperature from T_1 to T_2, is given simply by:

$$t_s = \frac{CSZ}{s} \tag{Eq. 10}$$

13

The time t_s is thus proportional to $\frac{Q}{s}$ (in 3D) and $\frac{Q^2}{s^2}$ (in 2D). This time corresponds to the time available for backfilling, i.e. liquid feeding of the opening mushy. Consequently, different solidification cracking behaviors are expected when changing welding conditions because of the associated changes in CSZ lengths and available backfilling time.

F. Shifting of stress cells

The non-uniform thermal distribution in and around the weldment during welding generates stress and strain gradients that affect solidification crack formation. A tensile cell favors cracking while a compressive cell hinders cracking. The stress-strain patterns formed during welding result from the non-uniform distribution of heat within the metal, with the net effect being localized deformation near the weld [63,64]. Compression and tensile stress cells exist around the moving weld pool as the magnitude of thermal stresses is quantified as the stress required to suppress thermal expansion or contraction. These cells are formed by thermally-induced dilatation gradients and solidification shrinkage (differential dilatation and contraction of the weld) [65]. They are shifted when varying welding speed thus modifying the nature (compression or tensile) of the cell around the mushy zone itself.

Experimental studies on dynamic plastic strains during GTA welding (Figure 12) have reported the possibility of a compressive cell at the trailing edge of the weld pool [63,66]. These cells depend on the temperature distribution around the weld pool. In stationary spot GTA welds, welding heat flow consists of concentric circle isotherms. The heated metal surrounding the stationary heat source is restrained by the cooler metal away from the heat source and therefore is in compression. The stress pattern is uniform. However, in case of a moving heat source, the asymmetric temperature distribution along the longitudinal axis generates compressive stresses of higher magnitude in front than behind the weld pool [63]. When plastic flow occurs, there will be a shifting of metal so as to reduce the unbalanced front-to-rear stress pattern [63].
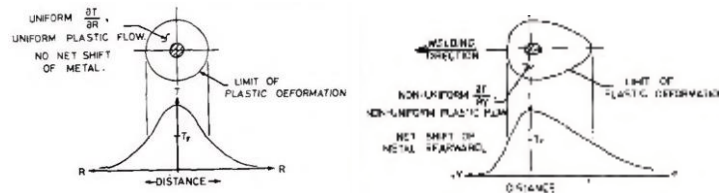

Figure 12   Comparison of thermal effects for (a) stationary and (b) moving heat source [63].

Chihoski attempted to resolve the stress field state around a moving weld pool [66]. The thermal stress pattern behind the weld pool (Figure 13) was compressive largely due to the plastic

flow of material from the front to the back. Further behind the weld pool, the stress changed from compressive to tensile (new tensile cell T_2) as both solidification shrinkage and cooling contraction lead to the development of tensile stresses as temperatures and temperature gradients decrease. It demonstrated that changing travel speed brought changes in the extent and magnitude of the stress fields and the location of transition from compressive to tensile. At slow travel speeds, the tensile cells T_s and T_2 combine and dominate behind the weld pool. The cracking susceptibility is high. In the opposite case, fast travel speeds tend to reduce compressive cell C_1 and shift the compressive cell C_2 toward the mushy zone, thus reducing the solidification crack susceptibility. The compressive cell C_2 can attain very high magnitudes [63]. These observations have been performed on partial-penetration, autogenous GTA aluminum welds at constant current (I = 280A) and varying welding speed (from 2.4 to 8.4 mm·s⁻¹) therefore at varying $\frac{Q}{s}$ ratio [66]. Note that these cells are mostly composed of transverse rather than longitudinal stresses. Thermo-mechanical modeling of welding using finite element method has later confirmed contractions of the fusion line in the neighborhood of the weld pool [64,67]. In case of a constant weld bead size, greater plastic flow regions and thus higher rearward plastic deformations are present behind a weld pool for faster welding speeds [63].
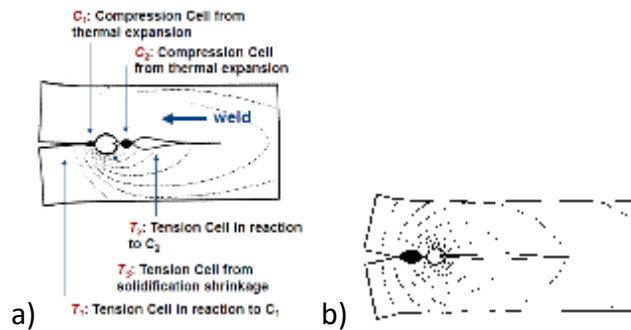

Figure 13   In-situ measurement of tensile and compressive cells surrounding the weld pool: (a) fast and (b) slow welding speeds [66]

Later Johnson measured strains using a moiré-fringe strain analysis technique around autogenous GTA welds on 3 mm-thick aluminum alloy sheets [63]. While Chihoski focused on transverse and longitudinal normal strains [66], Johnson's results indicate that the straining around the arc consists mostly of shear strains that increase with increasing current and welding speed [63]. The planes of maximum shear strain along the weldment side are oriented almost perpendicular and parallel to the weld bead whatever the welding parameters are. As welding speed and current increase, there is a marked increase in the temperature gradients ahead of the weld pool [63]. As welding speed increases (3.3 to 13.3 mm·s⁻¹) at constant penetration (i.e. iso-geometry of cross-sections), temperature gradients are greater in the transverse direction [63]. Subsequently the maximum temperature of a point near the weld will be lower, i.e. greater temperature gradients (Table 2) for faster welding speeds [63]. The restraint effect may shift the

stress pattern by limiting the expansion (hence increasing the compressive stresses) [68–70]. Moreover, as welding speed increases, the shear strain is increasingly confined to the immediate vicinity of the weld and shifted towards the weld rearwards [63].

Table 2 Temperature gradients in vicinity of partial penetration, GTA weld of Al-Mg alloy [63].

Travel Speed (mm·s⁻¹)	Current (A)	Temperature Gradient (°C/mm)			
		In front of Arc	10 mm behind arc	20 mm behind arc	30 mm behind arc
3.3	105	+20	-6	-4	-2
13.3	250	+30	-7	-5	-4

This shift has also been observed by Morgan-Warren and Jordan [59] as shown in the graph of the Linear Heat Content (LHC) calculated as:

$$LHC = \int T dy \qquad \text{(Eq. 11)}$$

, where y is the lateral distance from weld centerline. LHC values are mapped as a function of position (ξ) along the weld (Figure 14). The peaks of the curves indicate the point at which overall cooling and hence contraction of the parent metal begins. At fast travel speeds, the tensile cell is shifted behind the end of the mushy zone and therefore no cracking forms. Translating these results into strain and stress, it is found that faster welding speeds reduced the overall level of strain-stress and displaced away from the weld pool rear the tensile part induced by contraction [59]. The CSZ is therefore in a compression cell at fast travel speeds.
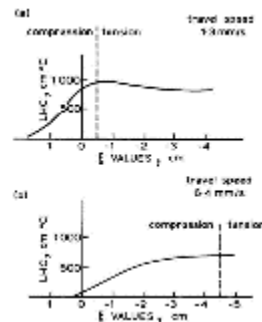

Figure 14 longitudinal distribution of LHC and associated compression and tensile force cells for GTA low-alloy steel welds of 3 mm sheets at (a) slow and (b) fast welding speeds [59].

Modeling the stress fields behind the weld pool in the Sigmajig testing (Figure 15) aimed at understanding the influence of dynamic stresses, induced by thermal and mechanical loading, on weld metal solidification crack formation [10]. These calculations are based on a mathematical model for arc welding processes that account for conduction and convection modes for heat transfer, buoyancy, electromagnetic forces, and surface tension gradients [60]. Dynamic mechanical factors are influenced by both restraint and welding parameters. A tensile stress

surrounding the mushy zone at the weld trailing edge creates a favorable condition for solidification crack formation as observed during full-penetration autogenous GTA welding of Type 316 austenitic stainless steel (Figure 16). A compressive cell behind the weld pool should hinder the formation of solidification cracking if surrounding entirely the mushy zone [10] but may not prevent it, as solidification cracking can form in highly susceptible microstructures under compressive stresses [19,28] because the compressive stress may not compensate the entire tension generated during solidification shrinkage on liquid films. Numerical simulations have confirmed the compressive and tensile stress fields changeovers along the weldment and their variations with travel speed [10].
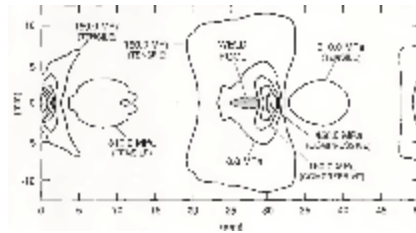

Figure 15   calculated stress distribution in Sigmajig test specimen for Type 316 SS GTA welds after 4s of welding and a pre-applied stress of 172 MPa [10].
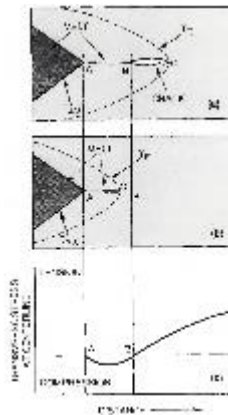

Figure 16   Relationship between (a,b) mushy zone extent and (c) compressive and tensile stress fields in case of solidification crack (a) formation or (b) avoidance [10]

G. Summary

The effect of travel speed on solidification cracking formation is not straightforward. Indeed, increasing travel speed results in opposing effects. It enhances the formation of solidification cracking by decreasing the centerline temperature gradient G, increasing the CSZ length,

decreasing the time to feed shrinkage, and generating centerline grain segregation. On the other hand, increasing travel speed hinders solidification crack formation by shifting the compression cell to the mushy zone, reducing the time exposed to strain, and refining weld metal grains. In summary, the travel speed influences solidification cracking formation through both thermal and metallurgical effects. Interestingly, Rosenthal modeling highlights that the welding speed affects differently the solidification cracking behavior depending on two welding conditions: is the welding speed s increased at constant welding power Q or constant ratio $\frac{Q}{s}$? Is the weld deposited in partial or full penetration? Part II of the review will focus on classifying the observed effects on solidification cracking behavior to the experimental welding conditions and metrics.

H. REFERENCES

[1]   T.C. Nguyen, D.C. Weckman, D.A. Johnson, H.W. Kerr, High speed fusion weld bead defects, Sci. Technol. Weld. Join. 11 (2006) 618–633. https://doi.org/10.1179/174329306X128464.

[2]   T.C. Nguyen, D.C. Weckman, D.A. Johnson, H.W. Kerr, The humping phenomenon during high speed gas metal arc welding, Sci. Technol. Weld. Join. 10 (2005) 447–459. https://doi.org/10.1179/174329305X44134.

[3]   J. Campbell, Castings, Elsiever, 2003.

[4]   A. Niel, F. Deschaux-beaume, C. Bordreuil, G. Fras, J.-M. Drezet, Hot tearing test for TIG welding of aluminum alloys: application of a stress parallel to the fusion zone, in: Hot Crack. Phenom. Welds III, 2011: pp. 43–58. https://doi.org/10.1007/b139103.

[5]   W.I. Pumphrey, J.V. Lyons, Cracking during the casting and welding of the more common binary aluminum alloys, JIM. 74 (1948) 439–455.

[6]   S. Chen, G. Guillemot, C. Gandin, Three-dimensional cellular automaton finite element modeling of solidiication grain structures for arc-welding processes, Acta Mater. 115 (2016) 448–467. https://doi.org/10.1016/j.actamat.2016.05.011.

[7]   F. Matsuda, H. Nakagawa, K. Sorada, Dynamic Observation of Solidification and Solidification Cracking during Welding with Optical Microscopy (I), Trans. JWRI. (1982) 67–77.

[8]   W.F. Savage, A.H. Aronson, Preferred Orientation in the Weld Fusion Zone, Weld. J. 45 (1966) 85s-89s.

[9]   G.J. Davies, J.G. Garland, Solidification Structures and Properties of Fusion Welds, Int. Metall. Rev. 20 (1975) 83–108.

[10]   T. Zacharia, Dynamic Stresses in Weld Metal Hot Cracking, Weld. J. (1994) 164–172.

[11] S. Chen, X. Ye, D.K.L. Tsang, L. Jiang, K. Yu, C. Li, Z. Li, Welding solidification cracking susceptibility and behavior of a Ni-28W-6Cr alloy, J. Mater. Sci. Technol. 35 (2019) 29–35. https://doi.org/10.1016/j.jmst.2018.09.013.

[12] B.T. Alexandrov, J.C. Lippold, Relationship Between the Solidification Temperature Range and Weld Solidification Cracking Susceptibility of Stainless Steels and Ni-base Alloys, Weld. World. Doc. IX-21 (2005) 1–12.

[13] J.C. Lippold, Recent developments in weldability testing, Hot Crack. Phenom. Welds. (2005) 271–290. https://doi.org/10.1007/3-540-27460-X_14.

[14] O. Hunziker, D. Dye, R.C. Reed, On the Formation of a Centreline Grain Boundary During Fusion Welding, Acta Mater. 48 (2000) 4191–4201.

[15] J.N. DuPont, C.V. Robino, A.R. Marder, Modelling mushy zones in welds of multicomponent alloys: implications for solidification cracking, Sci. Technol. Weld. Join. 4 (1999) 1–14. https://doi.org/10.1179/stw.1999.4.1.1.

[16] P. Schempp, C.E. Cross, A. Pittner, G. Oder, R.S. Neumann, H. Rooch, I. Dorfel, W. Osterle, M. Rethmeier, Solidification of GTA Aluminum Weld Metal : Part I – Grain Morphology Dependent upon Alloy Composition and, Weld. J. 93 (2014) 53s-59s.

[17] C.D. Lundin, C.P.D. Chou, Hot Cracking Susceptibility of Austenitic Stainless Steel Weld Metals, Weld. Res. Counc. 289 (1983) 1–79. http://www.aws.org/wj/supplement/WJ_1982_03_s82.pdf.

[18] C. Hagenlocher, D. Weller, R. Weber, T. Graf, Analytical Description of the Influence of the Welding Parameters on the Hot Cracking Susceptibility of Laser Beam Welds in Aluminum Alloys, Metall. Mater. Trans. A. 50 (2019) 5174–5180. https://doi.org/10.1007/s11661-019-05430-7.

[19] N. Coniglio, C.E. Cross, Weld parameter and minor element effects on solidification crack initiation in aluminium, in: Hot Crack. Phenom. Welds II, 2008.

[20] M.J. Dvornak, R.H. Frost, L. Olson, The Weldability and Grain Refinement of Al-2.2Li-2.7Cu, Weld. J. 68 (1988) 327s-335s.

[21] M.G. Mousavi, C.E. Cross, Ø. Grong, Eﬀect of scandium and titanium – boron on grain refinement and hot cracking of aluminium alloy 7108, Sci. Technol. Weld. Join. 4 (2015) 381–388. https://doi.org/10.1179/136217199101538030.

[22] W.K.B. Marshall, Welding aluminum-magnesium alloys, Trans. Inst. Weld. (1945) 53–57.

[23] Y. Arata, F. Matsuda, K. Nakata, K. Shinozaki, Solidification crack susceptibility of aluminum alloy weld metals (Report II), Trans. JWRI. 6 (1977) 91–104.

[24] C. Hagenlocher, D. Weller, R. Weber, T. Graf, Reduction of the hot cracking susceptibility of laser beam welds in AlMgSi alloys by increasing the number of grain boundaries, Sci.

Technol. Weld. Join. (2018) 1–7. https://doi.org/10.1080/13621718.2018.1534775.

[25] J.M. Drezet, M.S.F. Lima, J.D. Wagnière, M. Rappaz, W. Kurz, Crack-free aluminium alloy welds using a twin laser process, Weld. World. 52 (2008) 87–94.

[26] S. Lin, C. Aliravci, M.O. Pekguleryuz, Hot-tear susceptibility of aluminum wrought alloys and the effect of grain refining, Metall. Mater. Trans. A Phys. Metall. Mater. Sci. 38 (2007) 1056–1068. https://doi.org/10.1007/s11661-007-9132-7.

[27] P. Schempp, Grain refinement in aluminium GTA welds, Technische Universitat Berlin, 2013.

[28] N. Coniglio, C.E. Cross, Mechanisms for solidification crack initiation and growth in aluminum welding, Metall. Mater. Trans. A. 40 (2009) 2718–2728. https://doi.org/10.1007/s11661-009-9964-4.

[29] N. Coniglio, C.E. Cross, Initiation and growth mechanisms for weld solidification cracking, Int. Mater. Rev. 58 (2013) 375–397. https://doi.org/10.1179/1743280413Y.0000000020.

[30] N. Coniglio, Aluminum Alloy Weldability : Identification of Weld Solidification Cracking Mechanisms through Novel Experimental Technique and Model Development, BAM, 2008.

[31] H.R.Z. Rajani, A.B. Phillion, 3D multi-scale multi-physics modelling of hot cracking in welding, Mater. Des. 144 (2018) 45–54. https://doi.org/10.1016/j.matdes.2018.02.007.

[32] N. Coniglio, C.E. Cross, Coherency and grain size effects on solidification crack growth in aluminum welds, Mater. Test. Join. Appl. 56 (2014) 583–590.

[33] M. Braccini, C. Martin, M. Suery, Relation Between mushy zone rheology and hot tearing phenomena in Al-Cu alloys, Model. Cast. Weld. Adv. Solidif. Process. IX. (2000) 18–24. papers3://publication/uuid/B3582EAE-4EBC-48C2-8D43-F45001DFB1A4.

[34] N. Coniglio, C.E. Cross, Weld parameter and minor element effects on solidification crack initiation in aluminium, in: Hot Crack. Phenom. Welds II, Springer, 2008: pp. 277–310.

[35] N. Ramanaiah, K.S. Rao, B. Guha, K.P. Rao, Effect of modified AA4043 filler on partially melted zone cracking of Al-alloy gas tungsten arc welds, Sci. Technol. 10 (2005) 591–596. https://doi.org/10.1179/174329305X57482.

[36] G. Madhusudhan Reddy, A.K. Mukhopadhyay, A. Sambasiva Rao, Influence of scandium on weldability of 7010 aluminium alloy, Sci. Technol. Weld. Join. 10 (2005) 432–441. https://doi.org/10.1179/174329305X29456.

[37] J.H. Dudas, F.R. Collins, Preventing Weld Cracks in High-Strength Aluminum Alloys, Weld. J. 45 (1966) 241s-249s.

[38] K.R. Ravi, S. Manivannan, G. Phanikumar, B.S. Murty, S. Sundarraj, Influence of Mg on grain refinement of near eutectic Al-Si alloys, Metall. Mater. Trans. A Phys. Metall. Mater. Sci. 42

(2011) 2028–2039. https://doi.org/10.1007/s11661-010-0600-0.

[39] M.G. Mousavi, M.J.M. Hermans, G. den Ouden, Effect of Electromagnetic Stirring on Hot Cracking Susceptibility of Aluminum Alloy Welds, in: JOM Int. Conf., 2001: pp. 176–183.

[40] N.S. Biradar, R. Raman, Investigation of Hot Cracking Behavior in Transverse Mechanically Arc Oscillated Autogenous AA2014 T6 TIG Welds, MeT; Mat. Trans. A. 43A (2012) 3179–3191. https://doi.org/10.1007/s11661-012-1126-4.

[41] Y. Arata, F. Matsuda, H. Nakagawa, S. Katayama, S. Ogata, Solidificatĺon Crack Susceptibility in Weld Metals of Fully Austenitic Stainless Steels (Report III), Trans. JWRI. 6 (1977) 37–46.

[42] Y. Wei, Z. Dong, R. Liu, Z. Dong, Modeling the Trans-Varestraint test with finite element method, Comput. Mater. Sci. 35 (2006) 84–91. https://doi.org/10.1016/j.commatsci.2005.03.007.

[43] K. Nakata, F. Matsuda, Evaluations of ductility characteristics and cracking susceptibility of Al alloys during welding, Trans. JWRI. 24 (1995) 83–94.

[44] F. Matsuda, H. Nakagawa, H. Kohmoto, Y. Honda, Y. Matsubara, Quantitative Evaluation of Solidification Brittleness of Weld Metal during Solidification by In-situ Observation and Measurement (Report II), Trans. JWRI. (1983) 73–80.

[45] T. Senda, T., Matsuda, F., Takano, G., Watanabe, K., Kobayashi, T., Matsuzaka, Fundamental investigations on solidification crack susceptibility for weld metals with trans-varestraint test, Trans. JWS. 2 (1971) 1–22. https://doi.org/10.2207/qjjws1943.41.709.

[46] T.W. Nelson, J.C. Lippold, W. Lin, W.A. Baeslack III, Evaluation of the Circular Patch Test for Assessing Weld Solidification Cracking , Part I Development of a Test Method, Weld. J. (1997) 110–119.

[47] W.F. Savage, C.D. Lundin, The Varestraint Test, Weld. J. 44 (1965) 433s-442s.

[48] N. Bailey, S.B. Jones, The Solidification Cracking of Ferritic Steel During Submerged Arc Welding, Weld. J. 57 (1978) 217s-231s.

[49] W.A. Baeslack III, D.D. Harwig, J.C. Lippold, Weldability Testing of AL-Mg-Si-Alloys, 1990.

[50] C. V. Robino, M. Reece, G.A. Knorovsky, J.N. DuPont, Z. Feng, Prediction of maximum crack length in longitudinal varestraint testing, ASM Proc. Int. Conf. Trends Weld. Res. 2005 (2005) 313–318.

[51] C. V Robino, M. Reece, G.A. Knorovsky, J.N. DuPont, Z. Feng, Prediction of Maximum Crack Length in Longitudinal Varestraint Testing, ASM Proc. Int. Conf. Trends Weld. Res. (2005) 313–318. papers3://publication/uuid/33CA970E-E705-4ED5-9186-31FE74E62377.

[52] D. Statharas, H. Atkinson, R.O.B. Thornton, Getting the Strain Under Control : Trans-Varestraint Tests for Hot Cracking Susceptibility, Metall. Mater. Trans. A. 50 (2019) 1748–

1762. https://doi.org/10.1007/s11661-019-05140-0.

[53]   F. Matsuda, K. Nakata, S. Harada, Moving characteristics of weld edges during solidification in relation to solidification cracking in GTA weld of aluminum alloy thin sheet, Trans. JWRI. 9 (1980) 83–93.

[54]   Y. Arata, F. Matsuda, K. Nakata, S. Katayama, Solidification Crack Susceptibility in Weld Metals of Fully Austenitic Steels (Report II) – Effect of Ferrite, P, S, C, Si, and Mn on Ductility Properties of Solidification Brittleness, Trans. JWRI. 6 (1977) 105–117.

[55]   Z. Feng, A. David, T. Zacharia, C.L. Tsai, Quantification of thermomechanical conditions for weld solidification cracking, Sci. Technol. Weld. Join. 2 (1997) 11–19. https://doi.org/10.1179/stw.1997.2.1.11.

[56]   Y. Arata, F. Matsuda, K. Nakata, K. Shinozaki, Solidification Crack Susceptibility of Aluminum Alloy Weld Metals (Report II) - Effect of Straining Rate on Cracking Threshold in Weld Metal During Solidification, Trans. JWRI. 6 (1977) 91–104.

[57]   F. Matsuda, H. Nakagawa, K. Nakata, H. Okada, The VDR cracking test for solidification crack susceptibility on weld metals and its application to aluminum alloys, Trans. JWRI. 8 (1979) 85–95.

[58]   H. Tamura, N. Kato, S. Ochiai, Y. Katagiri, Cracking Study of Aluminum Alloys by the Variable Tensile Strain Hot Cracking Test, Trans. JWS. 8 (1977) 16–22.

[59]   E.J. Morgan-Warren, M.F. Jordan, Effect of travel speed on solidification cracking in autogenous tungsten inert gas arc welding of low- alloy steel sheet, Met. Technol. (1976) 29–40. https://doi.org/10.1179/030716976803391421.

[60]   T. Zacharia, A.H. Eraslan, D.K. Aidun, S.A. David, Three-Dimensional Transient Model for Arc Welding Process, Metall. Trans. B. 20B (1989) 645–659.

[61]   V.D. Fachinotti, a Cardona, Semi-analytical solution of the thermal field induced by a moving double-ellipsoidal welding heat source in a semi-infinite body, Mec. Comput. XXVII (2008) 1519–1530. e:%5CBIBLIO%5CArticles%5CSemi-analyt-solution-thermal-field-moving-welding-heat_Fachinotti_2008.pdf.

[62]   J. Goldak, A. Chakravarti, M. Bibby, A new finite element model for welding heat sources, Metall. Trans. B. 15 (1984) 299–305. https://doi.org/10.1007/BF02667333.

[63]   B.Y.L. Johnson, Formation of Plastic Strains During Welding of Aluminum Alloys, Weld. J. 52 (1973) 298s-305s.

[64]   Z. Feng, A computational analysis of thermal and mechanical conditions for weld metal solidification cracking, Weld. World. 33 (1994) 340–347.

[65]   N.R. Mandal, C.V.N. Sundar, Analysis of Welding Shrinkage, Weld. J. (1997) 233–238.

[66] R.A. Chihoski, The Character of Stress Fields Around a Weld Arc Moving on Aluminum Sheet, Weld. J. 168 (1972) 9s-18s.

[67] Z. Feng, T. Zacharia, S. David, On the thermomechanical conditions for weld metal solidification cracking, in: Math. Model. Weld Phenom. 3, The Institute of Materials, 1996: pp. 114–148.

[68] G. Argawa, H. Gao, M. Armithalingam, M. Hermans, Study of Solidification Cracking Susceptibility during Laser Welding in an Advanced High Strength Automotive Steel, Metals (Basel). 8 (2018) 1–15. https://doi.org/10.3390/met8090673.

[69] C.E. Cross, T. Bollinghaus, The Effect of Restraint on Weld Solidification Cracking in Aluminum, Weld. World. 50 (2006) 51–54.

[70] Z. Sterjovski, C. Bayley, J. Donato, N. Lane, D. Lang, Weld-end solidification cracking in pulsed-tandem gas metal arc welding of naval steels, Weld. J. 93 (2014) 145–152.